PCCP

Ultrafast pre-solvated dodecane hole capture and subsequent damage of used nuclear fuel extraction ligands DEHBA, DEHiBA, HONTA, CMPO, HEH[EHP] and TBP

Journal:	*Physical Chemistry Chemical Physics*
Manuscript ID	CP-ART-03-2025-000914.R1
Article Type:	Paper
Date Submitted by the Author:	19-Mar-2025
Complete List of Authors:	Cook, Andrew; Brookhaven National Laboratory, Chemistry Division Deokar, Rupali; Brookhaven National Laboratory, Chemistry Division

ARTICLE

Ultrafast pre-solvated dodecane hole capture and subsequent damage of used nuclear fuel extraction ligands DEHBA, DEH*i*BA, HONTA, CMPO, HEH[EHP] and TBP

Received 00th January 20xx,
Accepted 00th January 20xx

DOI: 10.1039/x0xx00000x

Rupali G. Deokar[a] and Andrew R. Cook[a,*]

Two classes of used nuclear fuel (UNF) extraction ligands, amide (DEHBA, DEH*i*BA, HONTA) and organophosphorus (CMPO, HEH[EHP], TBP), were selected to study radiation induced damage at picosecond to nanosecond timescale using electron pulse radiolysis in *n*-dodecane (DD) and supported by quantum chemical calculations. Spectra after radiolysis of 200 mM extraction ligands were recorded in DD/0.3 M DCM. Absorption peaks at 365, 365, 400 and 387 nm in case of DEHBA, DEH*i*BA, HONTA and CMPO respectively are assigned to triplet excited states. Additional absorption peaks at 420, 460 and 600 nm of DEHBA, DEH*i*BA and HONTA respectively were identified as due to ligand radical cations. A concentration dependent absorption peak at 600 nm in the case of CMPO was observed and assigned due to a combination of $CMPO^{\bullet+}$, $(CMPO)_2^{\bullet+}$ and possibly a radical degradation product of CMPO. Weak absorption peaks at 650 and 550 nm in case of HEH[EHP] and TBP were observed and tentatively assigned to their radical cations. A two-component $DD^{\bullet+}$ decay in the presence of ligands was observed due to different ligand oxidation mechanisms: ultrafast capture of pre-solvated DD holes and diffusive capture of solvated DD holes. At high extraction ligand concentrations (> 100 mM), the majority of DD holes were captured via an ultrafast pre-solvated pathway in < 10 ps with C_{37} values of 389, 401, 270, 374, 458 and 340 mM for DEHBA, DEH*i*BA, HONTA, CMPO, HEH[EHP] and TBP respectively. Following ultrafast capture, the remainder of DD holes became solvated and were captured with k = (2.32 ± 0.13), (1.78 ± 0.12), (1.38 ± 0.2), (0.98 ± 0.081), (1.09 ± 0.08) and (1.77 ± 0.046) x 10^{10} for DEHBA, DEH*i*BA, HONTA, CMPO, HEH[EHP] and TBP respectively. Subsequent hole transfer from the extraction ligands$^{\bullet+}$ to the low IP solute tri-*p*-tolylamine (TTA) showed only 4-16% hole transfer most likely indicating ligand$^{\bullet+}$ degradation in 0.9-4.6 ns.

Introduction

Nuclear energy is the best alternative to produce large amounts of energy with net low carbon emission and air pollution. Technical reactor and political challenges aside, a key issue in nuclear energy is the safe and clean production of fuels and disposition of radioactive waste. The best way to reduce used nuclear fuel (UNF) waste is to utilize reprocessing methods to separate radioactive metals for separate disposal or even better for reuse. Liquid-liquid extraction is currently the most commonly used method to separate radioactive metals from UNF. This process uses a selective organic ligand in an organic solvent to extract radioactive metals from UNF waste dissolved in an acidic aqueous phase. Therefore, novel ligands having selectivity for different radioactive metals are of current interest. Along with selectivity, UNF extraction ligands must also maintain their extraction and subsequent stripping efficiencies in the presence of the intense radiation environment caused by the metals. Different extraction schemes have been developed using different ligands. Examples of some processes which uses amide and organophosphorus extraction ligands are as follows. The classic PUREX process recovers U(VI) and Pu(IV) using tributyl phosphate (TBP, Fig. 1) at 30 % by volume in kerosene[1-3]. TRUEX is an alternative to PUREX which uses TBP along with *n*-octyl(phenyl)-*N*,*N*-diisobutylcarbamoylmethyl phosphine oxide (CMPO, Fig. 1) in *n*-dodecane (DD)[4-6]. The Actinide Lanthanide Separation Process (ALSEP) uses a mixture of tetra-2-ethylhexyldiglycolamide (TEHDGA) or *N,N,N′,N′*-tetraoctyldiglycolamide (TODGA) and 2-ethylhexylphosphonic acid mono-2-ethylhexyl ester (HEH[EHP], Fig. 1) in DD for MA/Ln separations[7, 8]. Processes using organophosphorus extraction ligands (TBP, CMPO, HEH[EHP]) introduce additional complexities, as they do not adhere to CHON principle, which allows for complete incineration and thus minimization of the final waste.[9, 10] A proposed alternative class of extraction ligands are *N,N*-dialkyl monoamides[11, 12]. In particular *N,N*-di-(2-ethylhexyl)butyramide (DEHBA, Fig. 1) and *N,N*-di-2-ethylhexylisobutyramide (DEH*i*BA, Fig. 1) are anticipated as direct substitutes for TBP,[11, 13-15] as they produce better U(VI) and Pu(IV) separation and radiolytic stability compared to TBP. These ligands are also being considered for direct dissolution of

[a] *Brookhaven National Laboratory, Upton, NY, 11973, USA*

† Electronic Supplementary Information (ESI) available: Additional figures, tables, details as referenced in the text and calculated molecular geometries. See DOI: 10.1039/x0xx00000x

metal containing UNF in an effort to reduce aqueous wastes.[16] The SELECT process in MA/Ln separation uses hexa-*n*-octylnitrilo-triacetamide (HONTA, Fig. 1) as a promising CHON candidate under acidic conditions[17-19].

Due to the radiation produced by radioactive metals, the organic solvents and extraction ligands used undergo radiochemical damage, which typically decreases extraction efficiency and increases waste and the cost of separations. Reports have identified that a major source of ligand damage to extraction ligands is a combination of direct ligand ionization and indirect oxidation by charge transfer from solvent radical cations.[20-27] Most of the above-mentioned model processes use DD as the organic solvent (commonly called the diluent). The rate constants of $DD^{\bullet+}$ reacting with TODGA[27-29], DEHBA[23], DEH*i*BA[23], HONTA[25], CMPO[20], HEH[EHP][26] and TBP[23] were reported to be 2.38, 0.9, 1.1, 0.76, 1.3, 0.47 and 1.4 x 10^{10} $M^{-1}s^{-1}$ respectively, however the nature of the reaction was not typically proven; it was simply assumed to be hole transfer (HT) even though proton transfer (PT) was energetically viable as well. Note also that these rate constants were measured with low concentrations on the nanosecond timescale, thus can miss key processes operating at high concentrations relevant to typical extraction conditions. To test this regime, faster time resolution is required. Picosecond pulse radiolysis is far less common but can determine the nature of reactions when extraction ligands are present at large concentrations (up to 1 M for example), thus enables greater mechanistic understanding of radiation effects under real extraction conditions. Using this technique, we recently reported that at concentrations exceeding 100 mM, TODGA captures most DD holes prior to their solvation in < 10 ps.[27] This ultrafast hole capture mechanism can have different dependence on solute than normal diffusive capture,[30-32] and leaves few solvated $DD^{\bullet+}$ to oxidize TODGA at the reported rates. We further showed that following this ultrafast oxidation, $TODGA^{\bullet+}$ decomposed rapidly, within 2.6 ns (at 200 mM TODGA). Electronic structure calculations suggested this extraction ligand damage was likely the result of either PT from the weakened C–H bonds in the $TODGA^{\bullet+}$ backbone or rupture of the C–C=O bond of $TODGA^{\bullet+}$. This work concluded that the only way to avoid these mechanisms of TODGA degradation was to have high concentrations of other species in solution that can compete with TODGA for capture of ultrafast holes. Work is underway to test this idea.

This contribution builds on the picosecond pulse radiolysis work with TODGA and examines additional proposed amide and organophosphorus based extraction ligands introduced above. In all cases, these ligands are expected to be used at high concentration to maximize metal separation and organic phase useful lifetime. A key question in all cases is to what extent are such proposed extraction ligands oxidized by ultrafast capture of solvent holes? Further, can we determine if after ultrafast oxidation these ligands also degrade like TODGA? While this work only examines uncomplexed organic phase ligands without contact with an acidic aqueous phase, it provides important foundational knowledge needed for a full understanding of radiation induced damage during extraction of UNF. Here we report measurements with DEHBA, DEH*i*BA, HONTA, CMPO, HEH[EHP] and TBP in DD/0.3 M DCM. Absorption spectra are reported for samples containing 200 mM of extraction ligands after radiolysis, as most of the ligands' radical cation spectra in DD are not known. Hole attachment rate constants at low concentration as well as efficiencies for ultrafast hole capture are determined. As with the earlier TODGA study, we evaluate the lifetime of ligand radical cations by determination of their ability to transfer the hole to a lower IP solute, tri-*p*-tolyl amine (TTA).

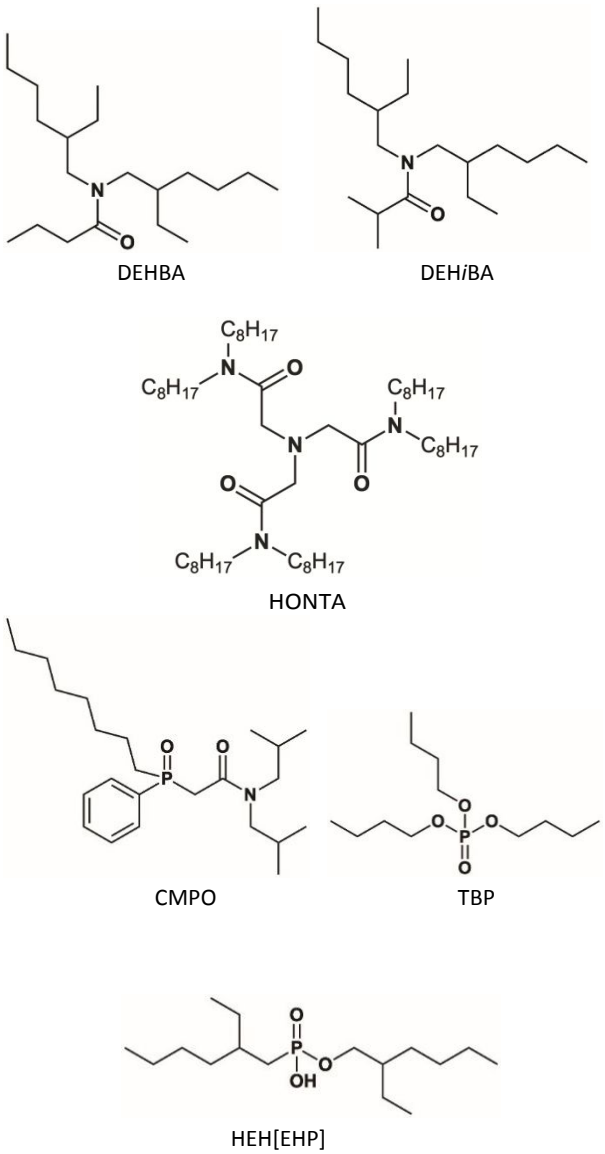

Fig. 1 Molecular structure of extraction ligands; *N,N*-di-(2-ethylhexyl)butyramide (DEHBA), *N,N*-di-2-ethylhexylisobutyramide (DEH*i*BA) and hexa-*n*-octylnitrilo-triacetamide (HONTA), *n*-octyl(phenyl)-N,N-diisobutylcarbamoylmethyl phosphine oxide (CMPO), 2-ethylhexylphosphonic acid mono-2-ethylhexyl ester (HEH[EHP]) and tributyl phosphate (TBP)

Materials and methods

DEHBA (99%) and DEH*i*BA (99%) were produced by Technocomm, ltd.. HONTA (96%) was custom made as previously reported.[25] CMPO (97%) and HEH[EHP] (98%) were purchased from Marshallton Labs. TBP (>99%) was purchased from Millipore Sigma. All extraction ligands were used as received. Tri-*p*-tolyl amine (98%) from TCI was used as received. Solvents, n-dodecane (DD, >99%) and dichloromethane (DCM, >99%) from Millipore Sigma were dried over 3A molecular sieves. Samples were sealed in custom made 0.5 cm pathlength Suprasil cells and degassed using argon. 0.3 M DCM was added to samples to scavenge electrons formed by ionization to reduce the rate of recombination in alkanes.

Picosecond electron pulse radiolysis experiments were performed at the Brookhaven National Laboratory Laser Electron Accelerator Facility (LEAF).[33] 9 MeV electron pulses of 5-10 ps duration were generated using UV photons from an ultrafast laser incident on a magnesium photocathode in an RF cavity. The output 3-5 nC electron pulses gave a dose of 10-20 Gy in samples, estimated by comparison to solvated electron absorption in a water sample. Data were normalized to the same dose using a Faraday cup. Transient absorption experiments with ~10 ps time resolution used the Optical Fiber Single-Shot (OFSS) detection system, described previously.[34] Briefly, the OFSS system utilizes a bundle of different length optical fibers that act as independent optical delay lines to collect complete transients with a 5 ns time window using a single electron pulse. 64 pulses were typically averaged to reduce noise. Data and spectra with ~1 ns time resolution were recorded using a pulsed xenon arc lamp (PTI Inc.), 10-25 nm bandwidth interference filters (Edmund Optics) and an FND-100Q silicon photodiode (EG&G), and digitized using a Teledyne LeCroy HDO6104-MS oscilloscope (1 GHz bandwidth, 12 bit vertical resolution, 2.5 GS/s). All data were collected and processed with LabView (National Instruments) and Igor Pro (Wavemetrics) software programs.

To support the experimental observations, quantum chemical calculations were performed using the Gaussian16[35] and GaussView[36] software packages. Calculations used the B3LYP functional[37, 38] and 6-31G(d,p) basis set[39], with solvation provided by the polarizable continuum model (IEFPCM) self-consistent reaction field (SCRF), using *n*-dodecane as the solvent (ε = 2.0060)[40]. Geometries were shown to be stable to a local minima using frequency analysis. IPs were calculated using enthalpies from frequency calculations. Free energies of reactions likewise used free energies from frequency calculations, and were further corrected for standard states.[41, 42] Time dependent density functional theory (TD)[43, 44] calculations were used to estimate the absorbance maximum (λ_{max}) of transient species.

Results and discussion

1. Transient absorption spectra of extraction ligands in DD

To our knowledge, the transient absorption spectra of selected extraction ligands in this study in DD have not been reported previously. The knowledge of formation of different transient species is crucial to understand the radiation chemistry of extraction ligands in organic solvents (diluents). In our previous findings,[27] due to a lack of a clear TODGA$^{\bullet+}$ absorption band, the nature and lifetime of TODGA$^{\bullet+}$ was deduced using other species. In this study we also wish to understand the nature of transient species formed after radiolysis of a wide variety of important proposed extraction ligands in DD, however found similar difficulties with most.

The radiolysis of alkanes,[45] such as DD used in this study, generates electrons (e^-), radical cations (DD$^{\bullet+}$), carbon centered radicals (DD(−H)$^{\bullet}$), hydrogen atoms (H$^{\bullet}$), and excited states (DD*):

$$DD \rightsquigarrow DD^{\bullet+}, e^-, DD(-H)^{\bullet}, H^{\bullet}, DD^* \quad (1)$$

The radiolytically generated e^- were scavenged by the well-known electron scavenger DCM (0.3 M)[46, 47]

$$CH_2Cl_2 + e^- \rightarrow {}^{\bullet}CH_2Cl + Cl^- \quad (2)$$

which also inhibits subsequent DD* formation from charge recombination.[48]

$$DD^{\bullet+} + e^- \rightarrow DD^* \quad (3)$$

H$^{\bullet}$ will seek out another radical or abstract H$^{\bullet}$ from the solvent, producing additional DD(−H)$^{\bullet}$. Under typical process conditions DD(−H)$^{\bullet}$ will react with oxygen to form largely inert peroxyl radicals, making DD$^{\bullet+}$ the most important radiolytically-induced oxidizing organic species.[21, 22, 24, 49] DD$^{\bullet+}$ can oxidize solutes having lower IP than DD. The calculated IP of DD in DD is 8.10 eV, and those for DEHBA, DEH*i*BA, HONTA and CMPO are 7.16, 6.84, 6.04 and 7.27 eV respectively and are thus all expected to be oxidized by DD$^{\bullet+}$. The IP values of HEH[EHP] and TBP, 8.24 and 8.34 eV respectively, are larger than that for DD, suggesting that they might not be oxidized or oxidized slowly due to entropy at the low concentrations produced. However, both HEH[EHP][26, 50] and TBP[51-53] are well known to form neutral dimers. The calculated IPs of HEH[EHP] and TBP dimers are 7.99 and 7.65 which are less than DD IP and therefore can be oxidized by DD$^{\bullet+}$. The calculated IPs of all species used in this report are provided in Table S1. The oxidation of ligands is an example of hole transfer from the solvent (HT, reaction 4). We note that like TODGA, calculations suggest that proton transfer to the ligands (PT, reaction 5) is also energetically favourable. We note that alkane radical cations are well known to lose a proton to suitable acceptors, such as provided by these extraction ligands. The computed free energies for both HT and PT are summarized in Table 1.

$$DD^{\bullet+} + \text{ligand} \rightarrow DD + \text{ligand}^{\bullet+} \quad (HT) \quad (4)$$
$$DD^{\bullet+} + \text{ligand} \rightarrow DD(-H)^{\bullet} + \text{ligand}(+H)^{+} \quad (PT) \quad (5)$$

The absorption spectra of most ligand$^{\bullet+}$ are not well known, thus spectra of 200 mM samples in DD/0.3 M DCM were recorded as a function of time after the electron pulse (SI Fig. S1a-S6a), with spectra at 3 ns after the electron pulse displayed in Fig. 2. The absorption peaks at 365, 365, 400 and 387 nm in the case of DEHBA, DEH*i*BA, HONTA and CMPO were quenched by O_2 and therefore identified due to triplet excited states (^{3}ligand*) (Fig. S1b-S6b). The long-lived ^{3}ligand* can be formed by both direct excitation (Reaction 6) and recombination with geminate electrons (Reaction 7),[54] though this reaction is largely blocked by the addition of DCM (Reaction 2).

ligand ⇝ e^- + ligand$^{\bullet+}$ + ^{3}ligands* (6)

ligands$^{\bullet+}$ + e^- → ligands* → ^{3}ligands* (7)

The second order rate constants for ligand triplet quenching were determined with O_2 saturated solutions ([O_2] ~10 mM in DD[55]) , with k = 2.6 x 10^8, 1.3 x 10^9, 2.6 x 10^8, and 9.3 x 10^8 M^{-1} s^{-1} for DEHBA, DEH*i*BA, HONTA, and CMPO respectively. All of these rate constants are below 1.3 x 10^9 M^{-1} s^{-1}. While they are expected to have small extinction coefficients, carbon centered radicals might also absorb, and will react with O_2, but typically at faster rates, in the range of 2–4 x 10^9 M^{-1} s^{-1} [56], thus are unlikely to contribute significantly to the observed peaks.

The absorption peaks at 420 nm in case of DEHBA and 460 nm in case of DEH*i*BA were neither quenched by O_2 (Fig. S1b and Fig. S2b) nor substantially concentration dependent (Fig. S1c and S2c) and therefore are assigned to DEHBA$^{\bullet+}$ and DEH*i*BA$^{\bullet+}$ respectively. TD-DFT calculations support the idea that DEHBA$^{\bullet+}$ and DEH*i*BA$^{\bullet+}$ absorb in the visible, though at redder wavelengths (Table S2). The absorption peaks at 420 and 460 nm of DEHBA and DEH*i*BA respectively decay leaving a 365 nm band (Fig. S1a and S2a), which is quenched by O_2 suggesting it is due to a ligand triplet. Moreover, experiments described in section 3 attempted to transfer any ligand captured holes to the lower IP (5.55 eV, Table S1) solute tri-*p*-tolylamine (TTA) (Fig. S7). Fig. S7 clearly indicates the absorbance at 420 nm and 460 nm were quenched by TTA, supporting the idea that these peaks are due to ligand$^{\bullet+}$.

Neat HONTA after radiolysis was reported to have an absorption peak at 400 nm assigned to ^{3}HONTA*, with a residual short-lived absorption from 500-900 nm likely due to HONTA$^{\bullet+}$.[25] Our experiments found similar results, but find a well resolved absorption peak at 600 nm that is not affected significantly by O_2 (Fig. S3b) nor by concentration (Fig. S3c) which ruled out the possibility of (HONTA)$_2^{\bullet+}$. This peak is thus assigned to HONTA$^{\bullet+}$. TD-DFT calculations are also consistent with this peak being HONTA$^{\bullet+}$ (Table S2). Moreover, the spectra of HONTA samples at different times shows that as the peak at 600 nm decreased, the peak at 400 nm increased (Fig. S3a), consistent with recombination making triplets.[57] It was suggested by Toigawa *et. al*[25], that this long time growth might be a result of HONTA$^{\bullet+}$ recombination with Cl^- (Reactions 8) having sufficient energy to make a triplet. The lack of such a growth with other ligands may suggest a lack of sufficient energy to make triplets in those cases (Fig. S3b).

[HONTA]$^{\bullet+}$ + Cl^- → ^{3}[HONTA]* + $Cl^{\bullet}$ (8)

CMPO also has a peak at 600 nm (Fig. 2, Fig. 4a), however this appears partly quenched by oxygen (Fig. S4b) making assignment of this band less clear. The rate constant was determined to be 1.53 x 10^{10} M^{-1} s^{-1} which is faster than determined for the triplet peak at 387 nm. It is unclear what this faster decay is due to and may be a combination of factors. The faster rate possibility indicates the existence of a CMPO radical degradation product which absorbs at 600 nm, and decays by reaction with O_2. Such a product may be generated by either proton transfer from CMPO$^{\bullet+}$ to a neutral CMPO and/or fragmentation of the CMPO$^{\bullet+}$ backbone:

CMPO$^{\bullet+}$ + CMPO → CMPO(−H)$^{\bullet}$ + CMPO(+H)$^+$ (9)

CMPO$^{\bullet+}$ → Backbone cleavage products (10)

Computations examined three different possible sites for proton transfer, but none of the radicals formed were predicted to have absorption near 600 nm (Tables S2, S3). Of possible backbone bond cleavages[5, 58] examined (Fig. S8), loss of an isobutyl side chain to yield a mono-isobutyl radical product was found to be energetically favourable and predicted to absorb at 455 nm, which might account for the part of the 600 nm band that decays with O_2. The part which was not quenched by O_2 is likely due to radical cation products. TD-DFT calculations give the absorption maxima of CMPO$^{\bullet+}$ at 455 nm. In addition, the 600 nm band increases at higher [CMPO] (Fig. S4c), suggesting production of dimer radical cations that also absorb. We note that $Cl^{\bullet}$ complexes with aromatics are known to absorb in the visible,[31, 59] but the spectrum is largely unchanged when DCM is omitted (Fig. S4d), so such a complex is unlikely a major contributor. Thus, the nature of the 600 nm band is probably complex, containing contributions from multiple species.

HEH[EHP] and TBP showed weak, featureless and broad absorption bands with peaks near 650 and 550 nm respectively (Fig. 2, Fig. S5a, Fig. S6a). Both of these bands were not quenched by O_2 (Fig. S5b and Fig. S6b), however decreased with increasing concentrations of HEH[EHP] and TBP (Fig. S5c and Fig. S6c). These peaks are most probably due to HEH[EHP]$^{\bullet+}$ and TBP$^{\bullet+}$ and possibly their dimer radical cations. The decrease in intensity with increasing concentration suggest either facile intermolecular proton transfer from the radical cation to a neutral ligand[60], production of ligand dimer cations that do not absorb strongly here, or simply more complete quenching of the underlying DD$^{\bullet+}$ absorbance at 600 nm. Absorption maxima calculated by TD-DFT again supports the idea of these radical cations absorbing in the visible region (874, 569, 568 and 477 nm for HEH[EHP]$^{\bullet+}$, (HEH[EHP])$_2^{\bullet+}$, TBP$^{\bullet+}$ and (TBP)$_2^{\bullet+}$ respectively). The absorbance of monomer and dimer radical cations in the visible region may be responsible for appearance of broad spectra in case of both HEH[EHP] and TBP. Wang *et al.*[60] reported a pure TBP spectrum using picosecond pulse radiolysis has a multi-component absorption band between 350 and 1500 nm, identifying the NIR component as solvated electrons. While they did not clearly identify TBP$^{\bullet+}$ absorption, the remainder of their spectrum is similar to that in Fig. S9.

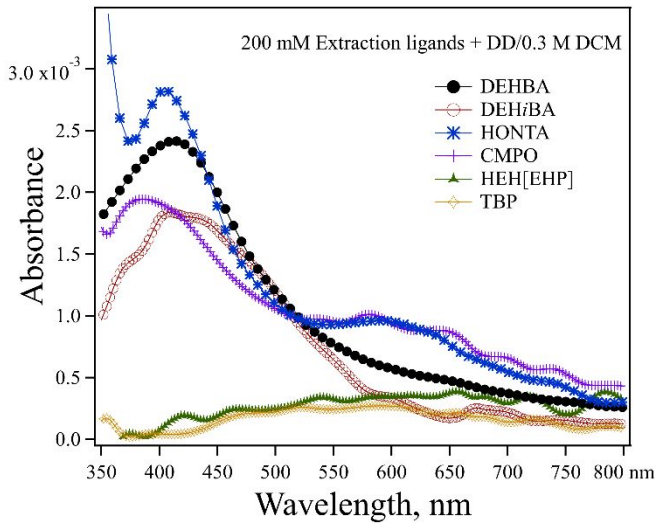

Fig. 2 Transient spectra obtained for electron pulse-irradiated, 200 mM samples of extraction ligands in DD/0.3 M DCM at 3 ns. The peaks at 365 nm in case of DEHBA and DEH*i*BA, 400 nm and 387 nm in case of HONTA and CMPO respectively are identified due to triplet excited states. The 420, 460 and 600 nm peaks of DEHBA, DEH*i*BA and HONTA respectively are identified as due to radical cations. The 600 nm peak in case of CMPO is more complex, possibly containing contributions from $CMPO^{\bullet+}$, $(CMPO)_2^{\bullet+}$ and radicals. Weak and broad absorption peaks at 650 and 550 nm in case of HEH[EHP] and TBP are likely due to a combination of monomer and dimer radical cations. Detailed time dependent spectra are provided in SI (Fig. S1a-S6a). Calculated absorption maxima are provided in Table S2.

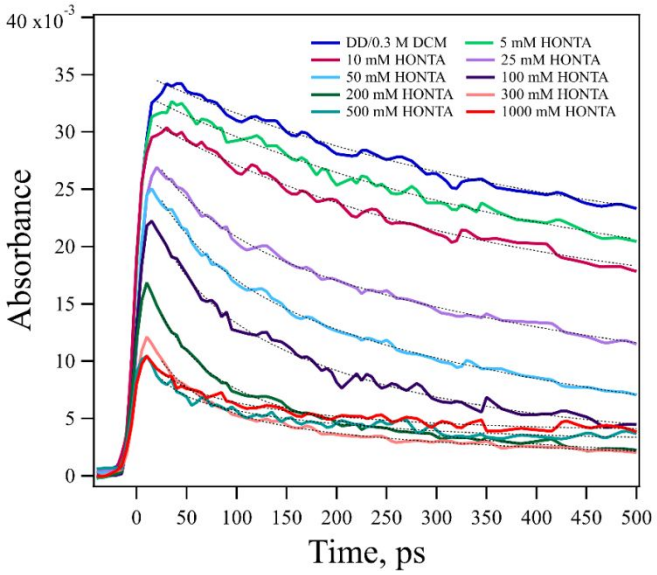

Fig. 3 Kinetic traces at 850 nm where $DD^{\bullet+}$ absorbs were obtained by OFSS after electron pulse irradiation, for 0–1000 mM HONTA in DD/0.3 M DCM. HT from $DD^{\bullet+}$ to HONTA after electron pulse radiolysis are described with a sudden component (~10 ps) followed by a resolved decay component, giving a rate constant of (1.38 ± 0.2) x 10^{10} M^{-1} s^{-1}.

2. Reaction mechanisms between $DD^{\bullet+}$ and extraction ligands

In this section we explore the kinetics and mechanisms of ligand oxidation following radiolysis. As described above, nearly all ligand radiolysis product absorptions are below 650 nm. The ligand radical cation absorptions identified above are generally weak and, in many cases, appear to be overlapped with other species. Because of this, it is more straightforward to determine the reaction kinetics between $DD^{\bullet+}$ and the ligands (Reaction 4) by watching the $DD^{\bullet+}$ absorption band decay as the hole is transferred. This can be monitored at 850 nm where $DD^{\bullet+}$ absorbs strongly (ε = 1.2 x 10^4 $M^{-1}cm^{-1}$, Fig. S10).[61] We note that while some ligand radical cations appear to absorb as far as 850 nm, these are weak tails and < 5% the magnitude of the absorption due to $DD^{\bullet+}$ so may be neglected. Transient absorption at 850 nm was recorded following pulse radiolysis for all ligands from 0-1000 mM. An example is shown in Fig. 3 for HONTA. Similar data for other ligands are shown in the SI, Fig. S11 (a)-(f).

The data has two key concentration dependent features: a well resolved decay preceded by a sudden loss of $DD^{\bullet+}$ faster than experimental time-resolution (~10 ps). The decays were fit in the same way as our recent report[27] with TODGA and used a double-exponential function (fits are dashed lines in Fig. 3). An attempt was made to fit kinetic traces using a single exponential decay, this did not adequately describe the non-exponential kinetics of geminate ion recombination that occurs after radiolysis. The rate constants from the dominant exponential are plotted against ligand concentration in Fig. 4. The second-order rate constants are finally determined by linear fits to these data using concentrations up to 100 mM to avoid possible dimer contributions at high concentrations. The values of rate constants for all extraction ligands are given in Table 1, along with previously reported values. The rate constant values from this work are slightly higher than previously reported values. The slight faster rates determined in this work may be due to the better time-resolution and may also be attributable to short-time enhancement of the apparent rate due to non-equilibrium effects when $DD^{\bullet+}$ is suddenly created, as reported previously.[62, 63]

The second order rate constants for DEHBA, DEH*i*BA, HONTA and CMPO do not include the impact of possible ligand dimer radical cation production, which is known for many species at high concentrations. Kinetic traces of DEHBA, DEH*i*BA and HONTA show anomalously slower decay at high concentration (especially 1 M), which might be an indication of dimer cation production and absorption overlapping at the same wavelength, so concentrations > 100 mM were not included in rate determinations. The same feature is not present for CMPO, HEH[EHP] and TBP, but this may simply be due to dimer cations

that do not absorb at 850 nm. As mentioned at the beginning of section 1, HEH[EHP] and TBP are well known to form neutral dimers, which will have lower IP than their monomer counterparts, increasing likelihood that they are oxidized by $DD^{\bullet+}$. The reported dimer association constants (K_a) for HEH[EHP][50] and TBP[51] in DD are 5500 and 2.6 M^{-1} respectively. With these K_a values, 1 M HEH[EHP] and TBP contain 99% and 65% dimers. The rate constants above for HEH[EHP] and TBP were determined after correcting solute concentrations for dimers, and assumed that both monomers and dimers react with $DD^{\bullet+}$ at the same rate. While considering the dimer concentration alone for HEH[EHP] gives about the same rate, for TBP using the concentration of dimers alone yielded an unrealistically high rate. We conclude that either the HT reaction with TBP monomer proceeds despite the predicted slightly endothermic energetics, or the reaction rate includes some amount of PT to monomers. To our knowledge, K_a values for other extraction ligands are unknown and therefore rates were not corrected for dimerization.

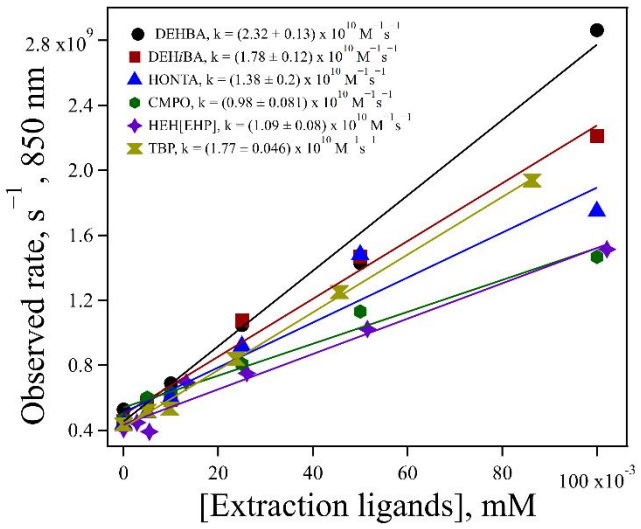

Fig. 4 Second-order rate constant plot for reaction of $DD^{\bullet+}$ with extraction ligands in DD/0.3 M DCM at 850 nm and 295 K. Solid line is weighted linear fit, corresponding to a slope of (2.32 ± 0.13), (1.78 ± 0.12), (1.38 ± 0.2), (0.98 ± 0.081), (1.09 ± 0.08) and (1.77 ± 0.046) x 10^{10} for DEHBA, DEH*i*BA, HONTA, CMPO, HEH[EHP] and TBP respectively. HEH[EHP] and TBP concentrations are corrected for dimers.

While these reaction rates are useful, a more important feature particularly at concentrations exceeding 100 mM is the apparent loss of $DD^{\bullet+}$ absorption at early times. This is seen in Fig. 3 and Fig. S11 (a)-(f) as the height of each trace at t=0. This loss of absorption as ligand concentration increased is due to a combination of direct solute ionization rather than the solvent and ultrafast hole transfer to the ligand, faster than the ~10 ps resolution of experiments. Note that PT on this timescale is unlikely as it involves mass transport. The observed ultrafast HT is important at high solute concentration, such as typically used for extraction ligands, and is not determined by the rate constants in Table 1. Rather, it is caused by capture of more reactive DD holes prior to solvation, when they can be captured much faster by mechanisms that are not well understood. This has been reported previously in chlorform[31 63], THF[30], water[64, 65] and dodecane[27, 66]. Direct ionization of extraction ligands can be calculated using the fraction of the total electron density of the sample due to extraction ligands (FED, Table S4). Note that the fraction of direct ligand ionization is large at 1 M, on average 38%, except for HONTA which is 96%.

In previous work, the fraction of solvent holes that were captured faster than solvation was well characterized using the exponential function in equation 10, to yield a concentration at which 37% of holes survive capture (C_{37}). This function was originally used by Hunt to describe pre-solvated electron capture in water[67, 68]:

$$f = 1 - \exp(-[S]/C_{37}) \quad (11)$$

where [S] is the ligand concentration. As only $DD^{\bullet+}$ absorbs in the current work, the absorbance of $DD^{\bullet+}$ at time=0 with various ligand concentrations can thus be written as the product of the absorption without ligand, the fraction of the electron density due to the solvent and the fraction of solvent holes that are not captured by solutes prior to solvation:

$$A_0([S]) = A_0([S]=0)(1-FED)e^{(-[S]/C_{37})} \quad (12)$$

Absorbance values A_0([S]) were determined by extrapolation of the data in Fig. S11 (a)-(f) to t=0 using an exponential fit over 20-500 ps. The signal magnitude was corrected for dose using a Faraday cup and relative sample densities to get signals corresponding to the same number of ionizations in all samples. A_0 values for the ligands are plotted in Figure 5 as a function of concentration. Fits with equation 11 determined C_{37} values (Table 1) for ultrafast hole transfer (< 10 ps) from $DD^{\bullet+}$ to ligands. Note that fits did not use 1 M data due to evidence for dimer radical cation absorption in some and also high direct ligand ionization. Finally, fits included a small residual absorption seen in both the neat solvent and ligand samples (Fig. S11 (a)-(f)) that was not due to $DD^{\bullet+}$. As mentioned above, C_{37} values of HEH[EHP] and TBP were corrected for dimerization of the neutral ligands. C_{37} values vary from 270 to 458 mM, with an average of 360 mM, close to the previously published value of 300 mM for TODGA.[27]

The import of ultrafast hole capture becomes more clear if we consider the fraction, f, of solvent holes captured. Values of f for 500 mM solutes are shown in Table 1. These values are large, suggesting that for most about 75% of the initial solvent radical cations are captured by this mechanism in << 10 ps. The fractions are lower for HEH[EHP] and TBP due to dimerization. When we also consider that at this concentration direct ionization accounts for about 20% (50% for HONTA) of the deposited dose, less than 20% of the $DD^{\bullet+}$ formed in a neat solvent sample survive to become solvated and have the chance to attach by diffusion. Note with higher ligand concentration, such as envisioned for direct dissolution conditions (e.g. 1.5 M

DEHBA and DEH*i*BA[16]) the fraction of holes that survive to attach by diffusion becomes vanishingly small, < 1%.

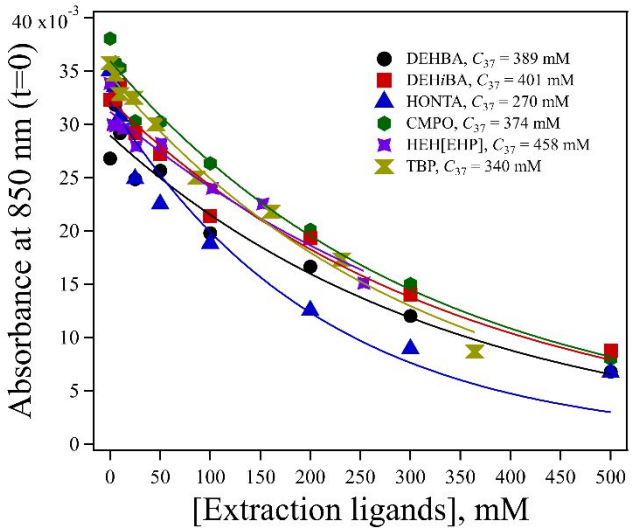

Fig. 5 The loss of $DD^{\bullet+}$ in the presence of DEHBA, DEH*i*BA, HONTA, CMPO, HEH[EHP] and TBP. Fits include consideration of both direct solute ionization and hole capture prior to solvation. The concentration at which 37% of solvent holes escape (C_{37}) pre-solvated hole capture and become solvated is 389, 401, 270, 374, 458 and 340 mM for DEHBA, DEH*i*BA, HONTA, CMPO, HEH[EHP] and TBP respectively.

Table 1 Summary of hole transfer reaction rates (reaction 4) from $DD^{\bullet+}$ to extraction ligands, with comparison to those previously reported in 0.3 M DCM/DD, computed free energies of HT and PT reactions between $DD^{\bullet+}$ and extraction ligands, C_{37} for pre-solvated hole capture, and fraction of $DD^{\bullet+}$ holes captured by 500 mM extraction ligands in under 10 ps.

Extraction ligand	*k*, (10^{10} $M^{-1}s^{-1}$), This work	*k*, (10^{10} $M^{-1}s^{-1}$), Previously reported	Δ*G* (eV) HT	Δ*G* (eV) PT	C_{37} (mM)	*f*
TODGA		2.38[27], 1.57[28, 29]	−1.02	−1.07	300	0.81
DEHBA	2.32 ± 0.13	0.90 [23]	-1.10	-0.96	389	0.72
DEH*i*BA	1.78 ± 0.12	1.10 [23]	-1.40	-1.00	401	0.71
HONTA	1.38 ± 0.2	0.76 [25]	-1.99	-1.96	270	0.84
CMPO	0.98 ± 0.081	1.30 [20]	-0.94	-1.26	374	0.74
HEH[EHP]	1.09 ± 0.08*	0.47* [26]	0.02	-0.54	458*	0.42*
TBP	1.77 ± 0.046*	1.40 [23]	0.11	-0.43	340*	0.66*

*Dimer corrected values

3. Are extraction ligands damaged rapidly after oxidation?

To investigate the stability of extraction ligand radical cations, experiments attempted to transfer holes captured by extraction ligands to the lower IP solute tri-*p*-tolylamine (TTA, IP = 5.55 eV, Table S1). TTA was selected because its radical cation is easily observed at 670 nm (Fig. S12) with a large ε = 26,200 $M^{-1}cm^{-1}$.[69] An inability to transfer holes is an indication of decomposition of ligand$^{\bullet+}$. In previous work, we showed that $TODGA^{\bullet+}$ only transferred ~10% of holes to TTA, indicating that 90% of $TODGA^{\bullet+}$ became damaged in 2.6 ns.[27] Conclusions were checked by comparison to *p*-xylene, which transferred all captured holes to TTA. HT reactions from all extraction ligands$^{\bullet+}$ in the current study to TTA are predicted to be energetically favourable (Table 2). For these tests, the concentration of extraction ligands was 200 mM except for HEH[EHP] and TBP which were increased to have a total of 200 mM monomers and dimers. The concentration of TTA used was 2 mM to initially transfer most $DD^{\bullet+}$ holes to the ligands and not to TTA. The low concentration of TTA allowed for most rapidly recombining geminate holes to decay before transfer to TTA. Measurements thus determined the concentration of homogeneous ions, i.e. free ions which escaped geminate pair recombination (free ion yield in DD ~ 0.1-0.2 / 100eV[70]). These $TTA^{\bullet+}$ decay slowly and are very easy to measure. While these ions are only a small fraction of all ions captured by the ligands, it is reasonable to assume that all radical cations captured by the ligands will undergo the same degradation processes (if any) as the homogeneous fraction of ions. Results are shown in fig. 6. In all cases the absorbance of $TTA^{\bullet+}$ produced when any of the ligands are present is much smaller than without the ligands. The data was analyzed by taking the ratio of the signals with ligand to that without at 100 ns, well after geminate recombination is complete. Note that the absorbance with ligands was first corrected for a small unknown absorbance in

samples with ligands only (Table S5). The absorption ratios give the fraction of holes transferred to TTA in the presence of ligands (f_{TTA}), and range from 0.037 to 0.16, as shown in Table 2. In previous work[27], we noted that Cl• atoms made after electron scavenging by DCM (also used here) followed by recombination produced extra TTA•+ but did not impact the ratios. We assume the same will hold here.

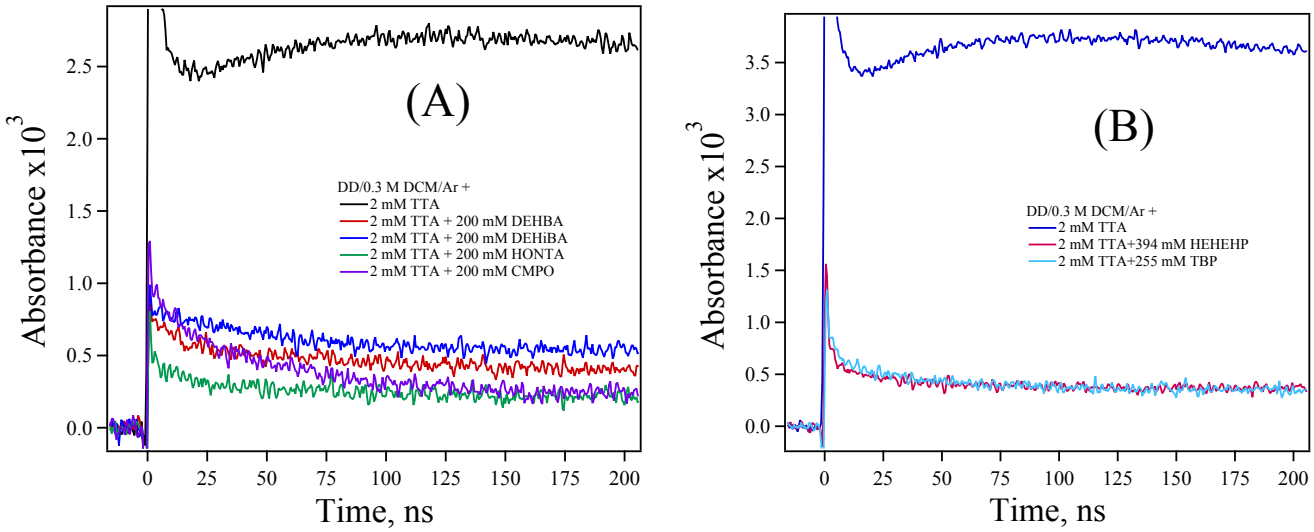

Fig. 6 Kinetic traces at 670 nm obtained for electron pulse-irradiated 2 mM TTA in the presence of a) 200 mM extraction ligands b) 394 mM HEH[EHP] and 255 mM TBP, in DD/0.3 M DCM, where samples were saturated with Ar. The concentrations of HEH[EHP] and TBP used are 394 and 255 mM respectively, to get final concentration (combination of monomer and dimer) of 200 mM.

As noted above, the most likely reason that few of the DD holes captured by ligands are passed to TTA is that the ligand•+ decomposes faster than the hole can be transferred. A concern might be that when and if ligand dimer radical cations form, they may stabilize the hole enough that it is uphill to pass to TTA. Calculations with HEH[EHP] and TBP suggested this was not the case, and we expect similar results if dimers of other ligand radical cations formed. Results indicate the ligand•+ degradation is large, finding that less than 4-16% survive long enough to pass their hole to TTA (Table 2). The lifetime of ligand•+ can be estimated by assuming that decomposition is in competition with hole transfer to TTA. The fraction of holes transferred to TTA (f_{TTA}) can thus be written as:

$$f_{TTA} = {[TTA]*k_{HT}}/{([TTA]*k_{HT}+k_{deg})} \quad (13)$$

Where k_{HT} is the rate of hole transfer from ligand•+ to TTA, and k_{deg} is the degradation rate of ligand•+ (s^{-1}). While k_{HT} is not known, for the purposes of an estimate we assumed it was the same as the rate for the HT reaction from DD•+ to TTA (k = 2.1 x 10^{10} $M^{-1}s^{-1}$ determined from 800 nm DD•+ decay fits, Fig. S13). Using f_{TTA} from Table 2, we find k_{deg} ranges from 0.22 – 1.09 x 10^9 $M^{-1}s^{-1}$, and thus the lifetimes of ligand•+ are in the range of 4.6 – 0.9 ns (Table 2). Note that if the actual HT rate from ligands•+ to TTA is faster, this lifetime gets shorter, and vice-versa. The average lifetime of these extraction ligands is similar to that determined previously for TODGA•+. This may suggest that the mechanism of degradation is common to all ligand•+. In the previous work, data suggested that proton transfer from TODGA•+ to neutral TODGA molecules was important but was unable to rule out extraction ligand backbone scission in the radical cations. We might expect that with different backbones in the current study, that backbone scission probability and rates might be substantially different among the ligands tested here, especially when comparing amide and organophosphorus ligands. By contrast, the proton transfer mechanism might be expected to be more similar among the ligands (Table S3), where a C-H bond is weakened in ligand•+, and transfers to an oxygen or nitrogen lone pair of electrons on a neutral ligand. This mode of damage will be difficult to protect against. A possible approach might be to remove all C-H bonds in the region of the ligands where the hole resides, perhaps replacing hydrogens with other groups such as methyls, which was partially tested by Galán *et. al*[71, 72] in the case of TODGA which gave promising but not entirely clear results. While DEHBA and DEH*i*BA[73, 74], HONTA[25], CMPO[5, 58, 75], HEH[EHP][26, 76], and TBP[73, 77, 78] are well known to be damaged after radiolysis, it is generally not well known how or when this initial damage occurs. Here we have determined that initial damage occurs within a few ns.

Table 2 Summary of calculated free energies of HT by extraction ligand$^{\bullet+}$ to TTA, fraction of extraction ligand$^{\bullet+}$ holes transferred to TTA, degradation rate (k_{deg}, s^{-1}) and lifetime of extraction ligand$^{\bullet+}$.

Extraction ligand	ΔG (eV)	f_{TTA}	k_{deg} (s^{-1}) x 10^9	τ (ns)
TODGA[27]	−1.56	0.10	0.39	2.60
DEHBA	−1.58	0.16	0.22	4.64
DEH*i*BA	−1.27	0.14	0.25	4.01
HONTA	−0.79	0.04	1.09	0.92
CMPO	−1.74	0.04	1.01	0.99
HEH[EHP]	−2.69	0.09*	0.41*	2.46*
TBP	−2.78	0.08*	0.49*	2.06*

*Dimer corrected values

Summary and Conclusions

Picosecond electron pulse radiolysis has been used to record transient absorption spectra of 200 mM amide and organophosphorus UNF extraction ligands. Spectra of DEHBA, DEH*i*BA, HONTA and CMPO show an absorption peak at ~400 nm due to triplet excited states which was confirmed by O_2 quenching. Radical cations of DEHBA, DEH*i*BA and HONTA were observed at 420, 460 and 600 nm respectively which was neither quenched by O_2 nor concentration dependent. CMPO shows a concentration dependent peak at 600 nm which was partially quenched by oxygen and therefore assigned due to a combination of CMPO$^{\bullet+}$, $CMPO_2^{\bullet+}$ and possibly a CMPO radical. HEH[EHP] and TBP spectra have weak and broad absorption peaks at 650 and 550 nm respectively, most probably due to their radical cations as they were not quenched by O_2. Experiments determined ligand oxidation after radiolysis due to charge transfer from DD$^{\bullet+}$. The rates of reaction were (2.32 ± 0.13), (1.78 ± 0.12), (1.38 ± 0.2), (0.98 ± 0.081), (1.09 ± 0.08) and (1.77 ± 0.046) x 10^{10} $M^{-1}s^{-1}$ for DEHBA, DEH*i*BA, HONTA, CMPO, HEH[EHP] and TBP respectively. In addition, ultrafast hole transfer from DD$^{\bullet+}$ to the ligands was also found to oxidize solutes within experimental time-resolution. The concentration at which 37% of the DD$^{\bullet+}$ holes survive capture (C_{37}) at ~10 ps was found to be 389, 401, 270, 374, 458 and 340 mM for DEHBA, DEH*i*BA, HONTA, CMPO, HEH[EHP] and TBP respectively. The rates and C_{37} values were corrected for known dimerization of HEH[EHP] and TBP. Calculations suggested that oxidation of HEH[EHP] and TBP are slightly energetically unfavourable but results still show oxidation. This may be driven by entropy effects due to the μM concentrations of radical ions, but also may be attributed to dimer formation which reduces the IP and thus making reactions energetically favourable. We also note that in the case of ultrafast capture, the energy of the initial state is not known, but it is higher than the relaxed DD$^{\bullet+}$ used in computations. Ultimately ligand radical cations are determined to degrade within 0.92-4.64 ns, based on their very limited ability to transfer the holes to the lower-IP solute TTA.

This study provides key insights into the application of extraction ligands in highly radioactive environments caused by extracted radioactive metals. Ligands will typically be used at large concentration to maximize extraction and organic phase lifetime. A key finding is that while much effort in the literature is spent determining the rate of hole transfer from solvent radical cations to ligands, these are of limited value in understanding the chemistry of production systems. When concentrated, direct solute ionization and ultrafast hole capture will be the primary way ligands get oxidized, and few solvent radical cations will survive the first few picoseconds to react at determined rates. Furthermore, this rapid oxidation of ligands is found to be followed by degradation within a few nanoseconds. These findings highlight the difficulty of protecting ligands from damage – there is little opportunity for bimolecular reactions to compete. The best way to protect unmodified ligands from damage will be to keep them from being oxidized in the first place. Future work will focus on the extent to which co-solutes such as phase modifiers and aromatics in kerosene might be able to effectively compete for ultrafast hole capture with the ligands. Another approach to be explored is to block proton transfer from ligand$^{\bullet+}$ by substitution of protons that may be lost with groups like methyl (as tested by Galán *et. al*[71, 72]) or even chloride. While such ligand modifications may help understand damage mechanisms, clearly a difficulty is the impact on ligand function.

Author contributions

Rupali G. Deokar: Writing – original draft, Experiments, Data analysis, Methodology, quantum chemical calculations.

Andrew R. Cook: Writing & editing, Data analysis, Supervision, Project administration, Conceptualization.

Conflicts of interest

There are no conflicts to declare.

Data availability

Data from this publication will be openly available, within 30 days of publication, in machine-readable format at https://doi.org/10.5281/zenodo.14963205.

Acknowledgements

This work and use of the Laser Electron Accelerator Facility of the Accelerator Center for Energy Research at BNL, was supported by the U.S. Department of Energy (DOE), Office of Science, Office of Basic Energy Sciences, Division of Chemical Sciences, Geosciences and Biosciences under contract DE-SC0012704. We are grateful to Gregary Holmbeck (Idaho National Laboratory, USA) for scientific discussions and for supplying DEHBA and DEH*i*BA, and Tomohiro Toigawa (Japan Atomic Energy Agency, Japan) for supplying HONTA.

Notes and references

1. W. B. Lanham and T. C. Runion, *PUREX PROCESS FOR PLUTONIUM AND URANIUM RECOVERY*, United States, 1949.
2. W. W. Schulz, K. P. Bender, L. L. Burger and J. D. Navratil, *Science and technology of tributyl phosphate*, Baca Raton, FL (United States); CRC Press, Inc., United States, 1990.
3. O. J. Wick, *Plutonium Handbook: A Guide to Technology*, American nuclear society, 1980.
4. E. P. Horwitz and D. G. Kalina, *Solvent Extr. Ion Exch.*, 1984, **2**, 179-200.
5. B. J. Mincher, S. P. Mezyk, G. Elias, G. S. Groenewold, J. A. LaVerne, M. Nilsson, J. Pearson, N. C. Schmitt, R. D. Tillotson and L. G. Olson, *Solvent Extr. Ion Exch.*, 2014, **32**, 167-178.
6. E. Philip Horwitz, D. C. Kalina, H. Diamond, G. F. Vandegrift and W. W. Schulz, *Solvent Extr. Ion Exch.*, 1985, **3**, 75-109.
7. G. J. Lumetta, A. V. Gelis, J. C. Carter, C. M. Niver and M. R. Smoot, *Solvent Extr. Ion Exch.*, 2014, **32**, 333-347.
8. A. V. Gelis and G. J. Lumetta, *Ind. Eng. Chem. Res.*, 2014, **53**, 1624-1631.
9. R. European Commission: Directorate-General for, Innovation, M. Hudson and C. Madic, *High-level liquid waste partitioning by means of completely incinerable extractants*, Publications Office, 1998.
10. E. Macerata, E. Mossini, S. Scaravaggi, M. Mariani, A. Mele, W. Panzeri, N. Boubals, L. Berthon, M.-C. Charbonnel, F. Sansone, A. Arduini and A. Casnati, *J. Am. Chem. Soc.*, 2016, **138**, 7232-7235.
11. G. M. Gasparini and G. Grossi, *Solvent Extr. Ion Exch.*, 1986, **4**, 1233-1271.
12. K. McCann, J. A. Drader and J. C. Braley, *Sep. Purif. Rev.*, 2018, **47**, 49-65.
13. J. A. Drader, N. Boubals, B. Camès, D. Guillaumont, P. Guilbaud, G. Saint-Louis and L. Berthon, *Dalton Trans.*, 2018, **47**, 251-263.
14. T. L. Authen, B. E. Tekikachew, M. R. S. J. Foreman, A. Wilden and C. Ekberg, *J. Radioanal. Nucl. Chem.*, 2022, **331**, 5137-5145.
15. D. R. Prabhu, G. R. Mahajan and G. M. Nair, *J. Radioanal. Nucl. Chem.*, 1997, **224**, 113-117.
16. A. E. Kynman, A. N. Dang, T. S. Grimes, S. P. Mezyk, J. R. Wilbanks, C. A. Zarzana, R. G. Deokar, A. R. Cook, D. Boglaienko, G. B. Hall and G. P. Horne, *ACS Omega*, 2025, DOI: 10.1021/acsomega.4c08506.
17. Y. Ban, H. Suzuki, S. Hotoku, N. Tsutsui, Y. Tsubata and T. Matsumura, *Solvent Extr. Ion Exch.*, 2019, **37**, 489-499.
18. Y. Sasaki, Y. Tsubata, Y. Kitatsuji, Y. Sugo, N. Shirasu and Y. Morita, *Solvent Extr. Ion Exch.*, 2014, **32**, 179-188.
19. Y. Sasaki, Y. Tsubata, Y. Kitatsuji and Y. Morita, *Chem. Lett.*, 2013, **42**, 91-92.
20. S. P. Mezyk, B. J. Mincher, S. B. Dhiman, B. Layne and J. F. Wishart, *J. Radioanal. Nucl. Chem.*, 2016, **307**, 2445-2449.
21. C. A. Zarzana, G. S. Groenewold, B. J. Mincher, S. P. Mezyk, A. Wilden, H. Schmidt, G. Modolo, J. F. Wishart and A. R. Cook, *Solvent Extr. Ion Exch.*, 2015, **33**, 431-447.
22. A. Kimberlin, D. Guillaumont, S. Arpigny, B. Camès, P. Guilbaud, G. Saint-Louis, H. Galán and L. Berthon, *New J. Chem.*, 2021, **45**, 12479-12493.
23. C. Celis Barros, C. D. Pilgrim, A. R. Cook, S. P. Mezyk, T. S. Grimes and G. P. Horne, *Phys. Chem. Chem. Phys.*, 2021, **23**, 24589-24597.
24. S. P. Mezyk, G. P. Horne, B. J. Mincher, P. R. Zalupski, A. R. Cook and J. F. Wishart, *Procedia Chem.*, 2016, **21**, 61-65.
25. T. Toigawa, D. R. Peterman, D. S. Meeker, T. S. Grimes, P. R. Zalupski, S. P. Mezyk, A. R. Cook, S. Yamashita, Y. Kumagai, T. Matsumura and G. P. Horne, *Phys. Chem. Chem. Phys.*, 2021, **23**, 1343-1351.
26. S. P. Mezyk, M. Baxter, C. Celis-Barros, T. S. Grimes, P. R. Zalupski, C. Rae, C. A. Zarzana, A. R. Cook and G. P. Horne, *Dalton Trans.*, 2024, **53**, 6881-6891.
27. R. G. Deokar and A. R. Cook, *Phys. Chem. Chem. Phys.*, 2024, **26**, 29060-29069.
28. G. P. Horne, C. Celis-Barros, J. K. Conrad, T. S. Grimes, J. R. McLachlan, B. M. Rotermund, A. R. Cook and S. P. Mezyk, *Phys. Chem. Chem. Phys.*, 2024, DOI: 10.1039/D4CP90191F.
29. G. P. Horne, C. Celis-Barros, J. K. Conrad, T. S. Grimes, J. R. McLachlan, B. M. Rotermund, A. R. Cook and S. P. Mezyk, *Phys. Chem. Chem. Phys.*, 2023, **25**, 16404-16413.
30. A. R. Cook, *J. Phys. Chem. A*, 2021, **125**, 10189-10197.
31. M. J. Bird, A. R. Cook, M. Zamadar, S. Asaoka and J. R. Miller, *Phys. Chem. Chem. Phys.*, 2020, **22**, 14660-14670.
32. S. Tagawa, N. Hayashi, Y. Yoshida, M. Washio and Y. Tabata, *Rad. Phys. Chem.*, 1989, **34**, 503-511.
33. J. F. Wishart, A. R. Cook and J. R. Miller, *Rev. Sci. Instrum.*, 2004, **75**, 4359-4366.
34. A. R. Cook and Y. Shen, *Rev. Sci. Instrum.*, 2009, **80**, 073106.
35. M. J. Frisch, G. W. Trucks, H. B. Schlegel, G. E. Scuseria, M. A. Robb, J. R. Cheeseman, G. Scalmani, V. Barone, G. A. Petersson, H. Nakatsuji, X. Li, M. Caricato, A. V. Marenich, J. Bloino, B. G. Janesko, R. Gomperts, B. Mennucci, H. P. Hratchian, J. V. Ortiz, A. F. Izmaylov, J. L. Sonnenberg, Williams, F. Ding, F. Lipparini, F. Egidi, J. Goings, B. Peng, A. Petrone, T. Henderson, D. Ranasinghe, V. G. Zakrzewski, J. Gao, N. Rega, G. Zheng, W. Liang, M. Hada, M. Ehara, K. Toyota, R. Fukuda, J. Hasegawa, M. Ishida, T. Nakajima, Y. Honda, O. Kitao, H. Nakai, T. Vreven, K. Throssell, J. A. Montgomery Jr., J. E. Peralta, F. Ogliaro, M. J. Bearpark, J. J. Heyd, E. N. Brothers, K. N. Kudin, V. N. Staroverov, T. A. Keith, R. Kobayashi, J. Normand, K. Raghavachari, A. P. Rendell, J. C. Burant, S. S. Iyengar, J. Tomasi, M. Cossi, J. M. Millam, M. Klene, C. Adamo, R. Cammi, J. W. Ochterski, R. L. Martin, K. Morokuma, O. Farkas, J. B. Foresman and D. J. Fox, *Gaussian 16*, 2016.

36. T. K. Roy Dennington, and John Millam, *GaussView, Version 6.1.1,* , Semichem Inc., Shawnee Mission, KS., 2019.
37. C. Lee, W. Yang and R. G. Parr, *Phys. Rev. B Condens. Matter*, 1988, **37**, 785-789.
38. A. D. Becke, *J. Chem. Phys.*, 1993, **98**, 5648-5652.
39. M. M. Francl, W. J. Pietro, W. J. Hehre, J. S. Binkley, M. S. Gordon, D. J. DeFrees and J. A. Pople, *J. Chem. Phys.*, 1982, **77**, 3654-3665.
40. J. Tomasi, B. Mennucci and R. Cammi, *Chem. Rev.*, 2005, **105**, 2999-3094.
41. C. P. Kelly, C. J. Cramer and D. G. Truhlar, *J. Phys. Chem. B*, 2007, **111**, 408-422.
42. C. P. Kelly, C. J. Cramer and D. G. Truhlar, *J. Phys. Chem. B*, 2006, **110**, 16066-16081.
43. C. Adamo and D. Jacquemin, *Chem. Soc. Rev.*, 2013, **42**, 845-856.
44. A. D. Laurent, C. Adamo and D. Jacquemin, *Phys. Chem. Chem. Phys.*, 2014, **16**, 14334-14356.
45. D. W. Werst and A. D. Trifunac, *Radiat. Phys. Chem.*, 1993, **41**, 127-133.
46. I. M. Salih, T. Söylemez and T. I. Balkaş, *Radiat. Res.*, 1976, **67**, 235-243.
47. T. I. Balkaş, *Int. J. Radiat. Phys. Chem.*, 1972, **4**, 199-208.
48. A. Saeki, N. Yamamoto, Y. Yoshida and T. Kozawa, *J. Phys. Chem. A*, 2011, **115**, 10166-10173.
49. Y. Sugo, Y. Izumi, Y. Yoshida, S. Nishijima, Y. Sasaki, T. Kimura, T. Sekine and H. Kudo, *Radiat. Phys. Chem.*, 2007, **76**, 794-800.
50. A. Kimberlin and K. L. Nash, *Solvent Extr. Ion Exch.*, 2021, **39**, 38-55.
51. D. M. Petković, *J. Inorg. Nucl. Chem.*, 1968, **30**, 603-609.
52. Q. N. Vo, C. A. Hawkins, L. X. Dang, M. Nilsson and H. D. Nguyen, *J. Phys. Chem. B*, 2015, **119**, 1588-1597.
53. Q. N. Vo, J. L. Unangst, H. D. Nguyen and M. Nilsson, *J. Phys. Chem. B*, 2016, **120**, 6976-6984.
54. S. L. Murov, I. Carmichael and G. L. Hug, *Handbook of photochemistry*, Marcel Dekker, New York, 2nd , rev. and expanded edn., 1993.
55. W. Hayduk, *SOLUBILITY DATA SERIES: ETHENE*, Oxford University Press, Oxford, UK 1994.
56. C. v. Sonntag, P. Dowideit, X. Fang, R. Mertens, X. Pan, M. N. Schuchmann and H.-P. Schuchmann, *Water Sci. Technol.*, 1997, **35**, 9-15.
57. S. Samori, M. Hara, S. Tojo, M. Fujitsuka, S.-W. Yang, A. Elangovan, T.-I. Ho and T. Majima, *J. Phys. Chem. B*, 2005, **109**, 11735-11742.
58. B. J. Mincher, S. P. Mezyk and G. S. Groenewold, *Procedia Chem.*, 2016, **21**, 66-73.
59. V. A. Aver'yanov, S. E. Kirichenko and I. V. Khudyakov, *Bulletin of the Academy of Sciences of the USSR, Division of chemical science*, 1983, **32**, 241-246.
60. F. Wang, G. P. Horne, P. Pernot, P. Archirel and M. Mostafavi, *J. Phys. Chem. B*, 2018, **122**, 7134-7142.
61. R. Mehnert, O. Brede and W. Naumann, *J. Radioanal. Nucl. Chem.*, 1986, **101**, 307-318.
62. A. R. Cook, P. Sreearunothai, S. Asaoka and J. R. Miller, *J. Phys. Chem. A*, 2011, **115**, 11615-11623.
63. A. R. Cook, M. J. Bird, S. Asaoka and J. R. Miller, *J. Phys. Chem. A*, 2013, **117**, 7712-7720.
64. F. Wang, U. Schmidhammer, A. de La Lande and M. Mostafavi, *Phys. Chem. Chem. Phys.*, 2017, **19**, 2894-2899.
65. A. de la Lande, S. Denisov and M. Mostafavi, *Phys. Chem. Chem. Phys.*, 2021, **23**, 21148-21162.
66. T. Kondoh, J. Yang, K. Norizawa, K. Kan, T. Kozawa, A. Ogata, S. Tagawa and Y. Yoshida, *Radiat. Phys. Chem.*, 2013, **84**, 30-34.
67. R. K. Wolff, J. E. Aldrich, T. L. Penner and J. W. Hunt, *J. Phys. Chem.*, 1975, **79**, 210-219.
68. K. Y. Lam and J. W. Hunt, *Int. J. Radiat. Phys. Chem.*, 1975, **7**, 317-338.
69. I. R. Gould, D. Ege, J. E. Moser and S. Farid, *J. Am. Chem. Soc.*, 1990, **112**, 4290-4301.
70. A. O. Allen, *Yields of free ions formed in liquids by radiation*, United States, 1976.
71. H. Galán, C. A. Zarzana, A. Wilden, A. Núñez, H. Schmidt, R. J. M. Egberink, A. Leoncini, J. Cobos, W. Verboom, G. Modolo, G. S. Groenewold and B. J. Mincher, *Dalton Trans.*, 2015, **44**, 18049-18056.
72. V. Hubscher-Bruder, V. Mogilireddy, S. Michel, A. Leoncini, J. Huskens, W. Verboom, H. Galán, A. Núñez, J. Cobos, G. Modolo, A. Wilden, H. Schmidt, M. C. Charbonnel, P. Guilbaud and N. Boubals, *New J. Chem.*, 2017, **41**, 13700-13711.
73. Y. Wang, Y. Wan, Y. Cai, L. Yuan, W. Feng and N. Liu, *Radiochim. Acta*, 2021, **109**, 603-623.
74. G. P. Horne, S. P. Mezyk, B. J. Mincher, C. A. Zarzana, C. Rae, R. D. Tillotson, N. C. Schmitt, R. D. Ball, J. Ceder, M.-C. Charbonnel, P. Guilbaud, G. Saint-Louis and L. Berthon, *Radiat. Phys. Chem.*, 2020, **170**, 108608.
75. G. S. Groenewold, G. Elias, B. J. Mincher, S. P. Mezyk and J. A. LaVerne, *Talanta*, 2012, **99**, 909-917.
76. C. G. Bustillos, R. O. Ngelale and M. Nilsson, *Solvent Extr. Ion Exch.*, 2023, **41**, 449-482.
77. M. H. Lloyd and R. L. Fellows, *Alpha radiolysis and other factors affecting hydrolysis of tributyl phosphate*, United States, 1985.
78. A. Dodi and G. Verda, *J. Chromatogr. A*, 2001, **920**, 275-281.

Data from this publication will be openly available, within 30 days of publication, in machine-readable format at https://doi.org/10.5281/zenodo.14963205.